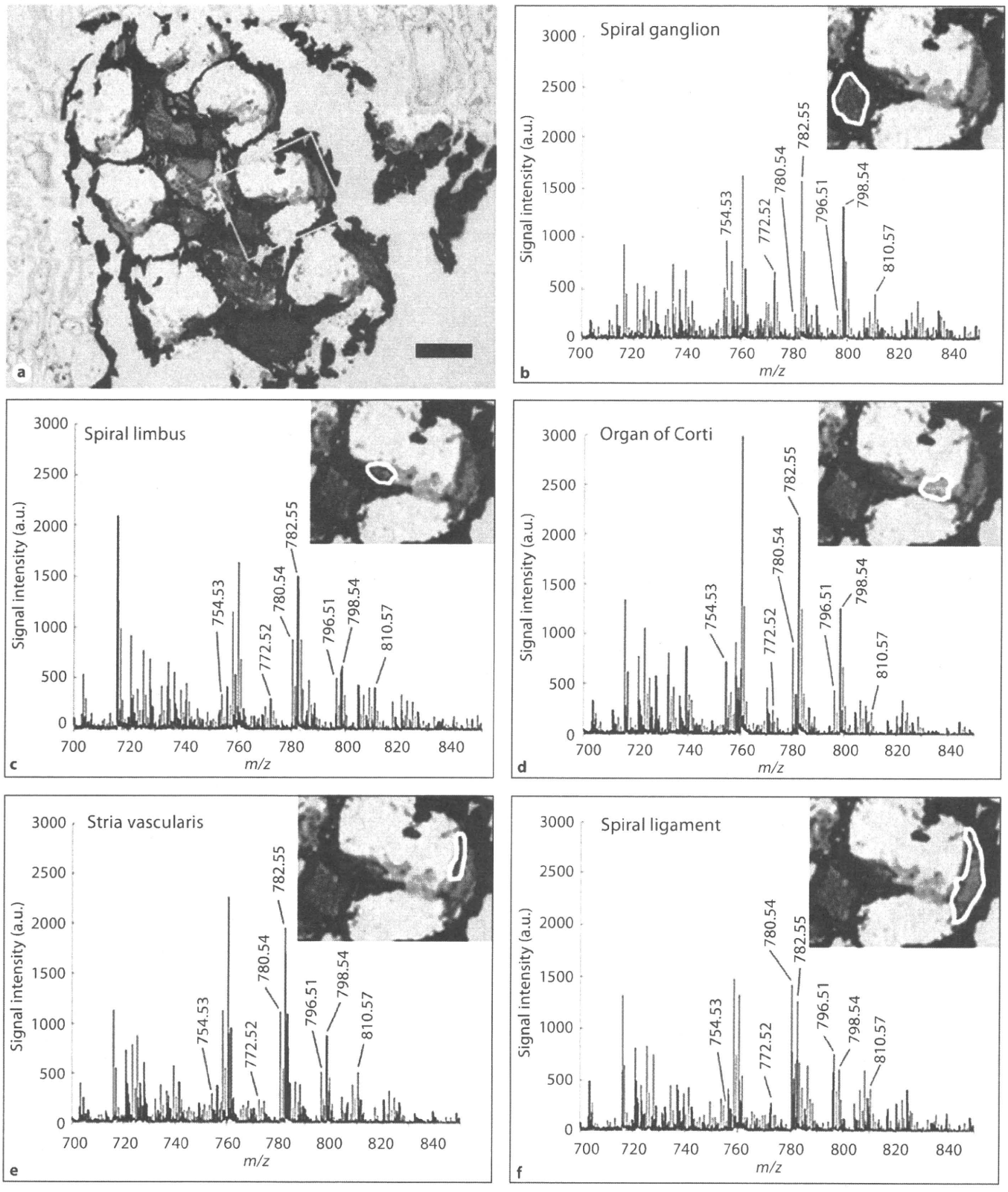
a
b
Spiral ganglion
Signal intensity (a.u.)
m/z
754.53
772.52
780.54
782.55
796.51
798.54
810.57
c
Spiral limbus
d
Organ of Corti
e
Stria vascularis
f
Spiral ligament

2

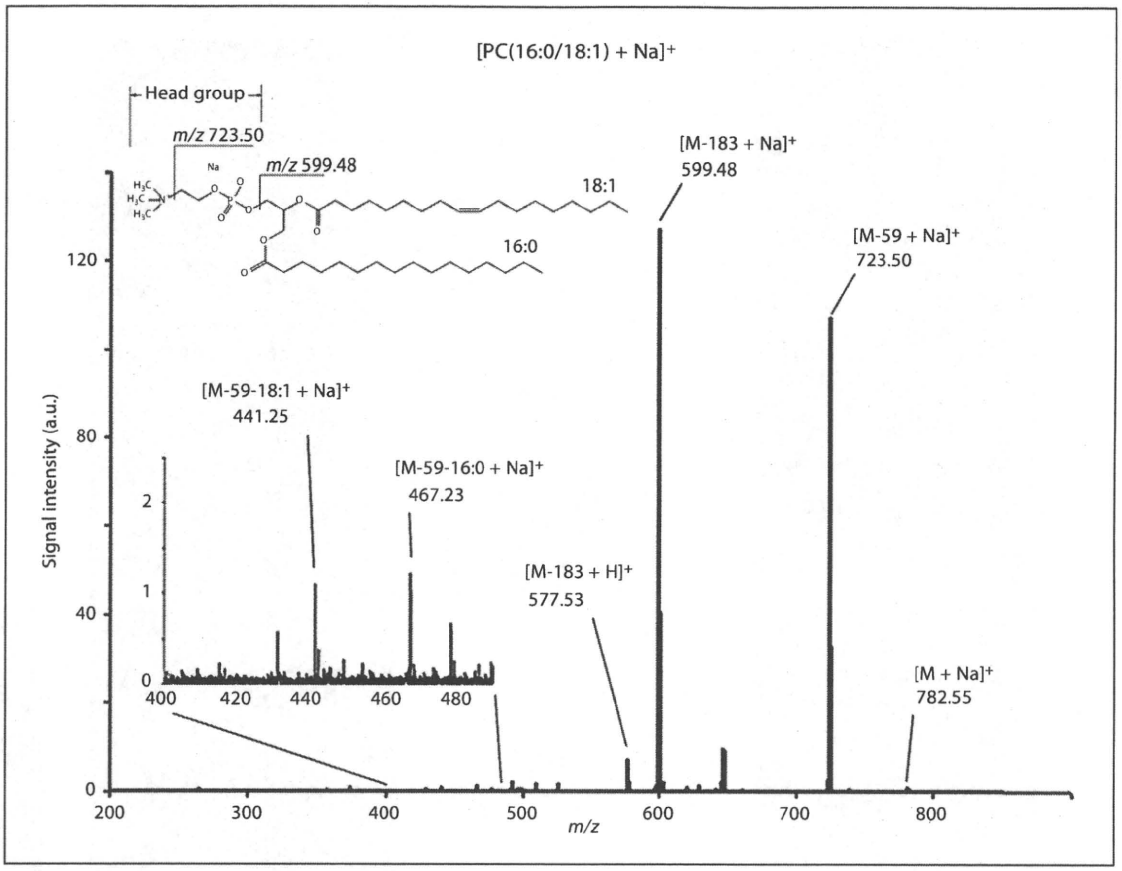

Fig. 3. MS/MS analysis for *m/z* 782.55. The structure of one peak was analyzed. The product ion spectrum of *m/z* 782.55 as a precursor ion was obtained by MS/MS analysis of a guinea pig cochlear section. This biomolecule was identified by neutral loss as $[PC(16:0/18:1) + Na]^+$.

differences can clearly be seen in the reconstructed mass images for each of the regions (fig. 4a–e). $[PC(16:0/16:0) + K]^+$ was predominantly found in the cochlear nerve in the modiolus and the neurons in the osseous spiral lamina (fig. 4a), while $[PC(16:0/16:1) + Na]^+$ was primarily located in the organ of Corti (fig. 4b). $[PC(16:0/18:1) + Na]^+$ was distributed mainly in the organ of Corti and the stria vascularis (fig. 4c). $[PC(16:0/18:2) + Na]^+$ was localized in the spiral ligament (fig. 4d), and $[PC(18:0/18:1) + Na]^+$ was distributed widely in the cochlea, but sparsely in the organ of Corti (fig. 4e). The Scheffé test was used to identify statistically significant differences among the regions. Differences in the localization of the PC species can clearly be seen in a merged image of PC(16:0/18:1) and PC(16:0/18:2) in figure 4f. In the lateral wall of the cochlear duct, the stria vascularis (red) and the spiral ligament (green) can easily be distinguished (fig. 4g).

Fig. 2. Photomicrograph of an unfixed cochlear section under the mass microscope and mass spectra from five regions of the cochlea. Prior to mass spectral analysis, a cochlear section was observed microscopically (**a**; bar = 500 μm). Mass spectra were obtained from the spiral ganglion (**b**), the spiral limbus (**c**), the organ of Corti (**d**), the stria vascularis (**e**), and the spiral ligament (**f**). **b–f Insets** correspond to the green square in **a**, with each region outlined in white.

Discussion

In recent years, MS has become a powerful tool for analyzing biomolecules, including those in the cochlea. Swan et al. [2009] analyzed mouse perilymph and determined the relative molar amounts of proteins in the perilymph and cerebrospinal fluid. Kathiresan et al. [2009] demonstrated that a large-conductance Ca^{2+}-activated

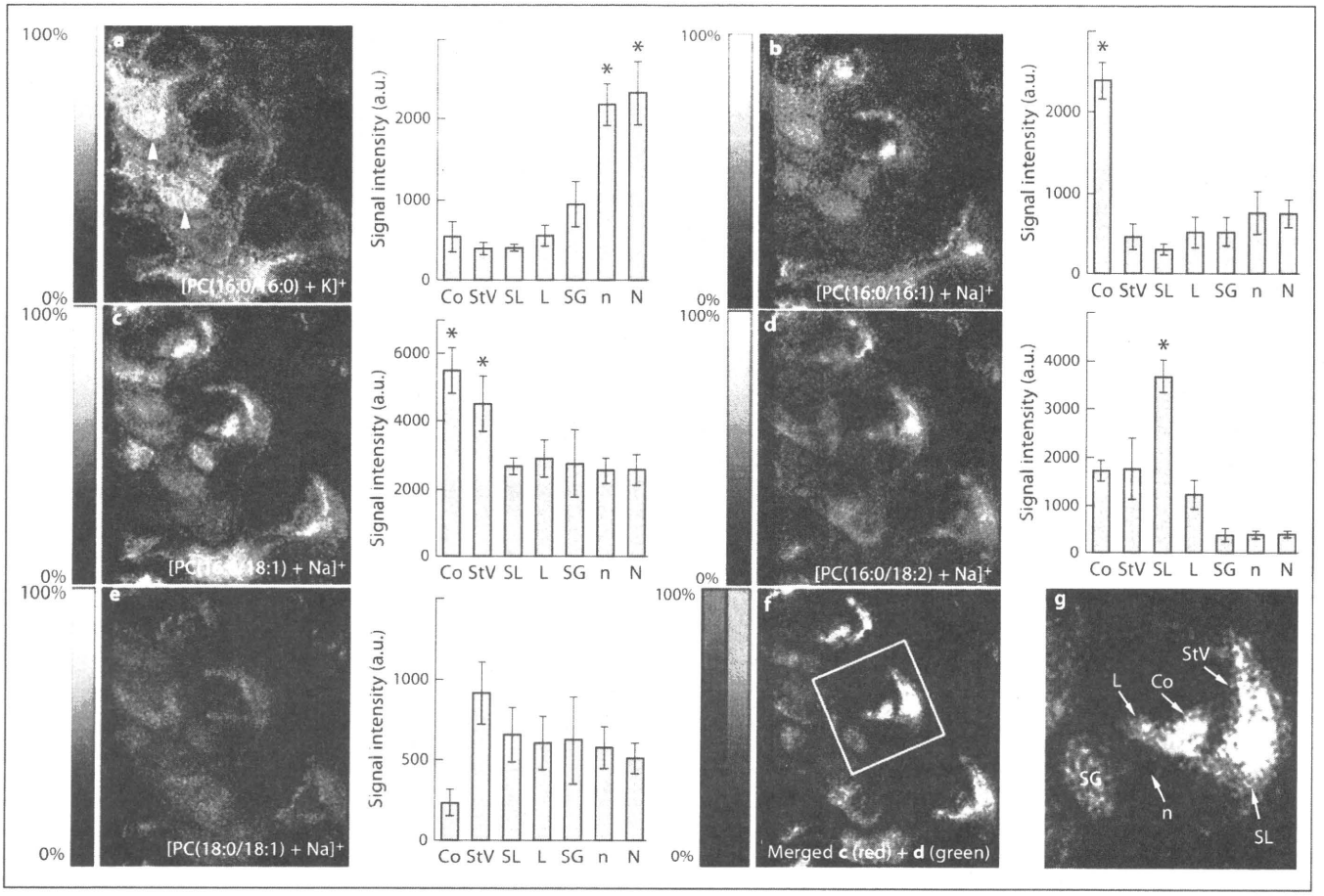

Fig. 4. Representative mass images showing the distributions of PC species identified by MS/MS analyses and the ion intensities in seven regions of the cochlea. **a** $[PC(16:0/16:0) + K]^+$ was predominantly found in the cochlear nerve in the modiolus (arrowheads) and the neurons in the osseous spiral lamina. **b** $[PC(16:0/16:1) + Na]^+$ was primarily found in the organ of Corti. **c** $[PC(16:0/18:1) + Na]^+$ was primarily found in the organ of Corti and the stria vascularis. **d** $[PC(16:0/18:2) + Na]^+$ was found in the spiral ligament. **e** $[PC(18:0/18:1) + Na]^+$ was widely distributed throughout the cochlea except in the organ of Corti. Statistically significant differences between the ion intensities for the region (marked) versus the other groups (unmarked) were determined using one-way analysis of variance followed by the Scheffé test. * $p < 0.05$ indicates a significant difference. Error bars indicate standard deviations. **f** Merged image of **c** (red: $[PC(16:0/18:1) + Na]^+$) and **d** (green: $[PC(16:0/18:2) + Na]^+$). **g** Higher magnification of the area indicated by the white square in **f**. The stria vascularis and the spiral ligament are clearly distinguishable by the differing distributions of PC species. Co = Organ of Corti; StV = stria vascularis; SL = spiral ligament; L = spiral limbus; SG = spiral ganglion; n = neurons in the osseous spiral lamina; N = cochlear nerve in the modiolus.

K^+ channel is associated with the protein interactome of the mouse cochlea. However, information on the localization of biomolecules was limited because samples needed to be homogenized for MS analyses.

IMS can be used to address this limitation. Lechene et al. [2006] obtained elegant atomic mass images of the cochlea without complicated pretreatment, such as those required for immunohistochemistry, radioisotope labeling, or in situ hybridization. However, these images were atomic mass images, which do not allow visualization of biomolecular localization. The present study demonstrated the use of mass microscopy to obtain mass images of biomolecules in the cochlea at a microscopic level.

In the present mass microscope [Harada et al., 2009], the spatial resolution of mass images was improved from 50 to 10 μm by focusing the laser size for ionization of biomolecules and increasing the sensitivity for detection of biomolecules in comparison to conventional MALDI-QIT-TOF-based IMS. Additionally, the mass microscope included an optical microscope, allowing us to observe

Table 1. Five groups (G) of PC species (a–e) identified by MS/MS analyses

G	PC species	Observed *m/z*	Calculated *m/z*	DMass[1]
a	PC(16:0/16:0) + K	772.527	772.5252	0.0027
b	PC(16:0/16:1) + Na	754.537	754.5357	0.0012
c	PC(16:0/18:1) + Na	782.552	782.5670	0.0150
	PC(16:0/18:1) + K	798.543	798.5409	0.0020
d	PC(16:0/18:2) + Na	780.547	780.5513	0.0043
	PC(16:0/18:2) + K	796.518	796.5252	0.0072
e	PC(18:0/18:1) + Na	810.579	810.5983	0.0183

PC(16:0/18:1) (c) and PC(16:0/18:2) (d) have two *m/z* values associated with different adducted ions (Na^+, K^+).

[1] The deviation of the observed *m/z* from the calculated *m/z*.

the sections and precisely select scan areas irradiated by the laser. Moreover, the QIT-TOF MS is suitable for precisely detecting low-molecular-weight biomolecules such as lipids. Therefore, this instrument enabled us to analyze the PC species in small and sophisticated organs like the cochlea. On the other hand, in the case of examinations for high-molecular-weight biomolecules like proteins, TOF/TOF MS seems to be suitable for identification [Yao et al., 2008].

In this study, we were able to clearly distinguish five PC species in individual regions of the cochlea, such as the spiral ganglion, the cochlear nerve, the spiral limbus, the organ of Corti, the stria vascularis, and the spiral ligament. PC species influence enzymes such as glutathione reductase and superoxide dismutase, which neutralize reactive oxygen species in the brain [Benzi et al., 1989]. On the other hand, in the cochlea, glutathione protects against noise-induced hearing loss [Yamasoba et al., 1998]. McFadden et al. [1999] demonstrated that age-related cochlear hair cell loss was enhanced in mice that carried a null mutation of the superoxide dismutase gene. Additionally, Seidman et al. [2002] reported that PC species preserved cochlear mitochondrial function and prevented age-related hearing loss. By affecting these processes, PC species play a crucial role in maintaining homeostasis in the cochlea, particularly in protecting from these stress reactions.

The activities of the five PC species, as identified by various binding patterns in the cochlear duct, can be examined with respect to their localizations in other organs that resemble the cochlea; specifically, the brain as a neuronal system and the kidney as an ion cycling system. In the brain, distribution patterns of PC species including PC(16:0/16:0) and PC(16:0/18:1) have been reported in the granular layer of the olfactory bulb, piriform cortex, insular cortex, and the molecular layer of the cerebellum. These layers are known to have areas high in neuronal plasticity [Mikawa et al., 2009]. In the present study, PC(16:0/16:0) was observed in the cochlear nerve in the modiolus and neurons in the osseous spiral lamina, and PC(16:0/18:1) was identified in the organ of Corti. Thus, these two PC species may be associated with neuronal systems. On the other hand, the intensity of PC(18:0/18:1) was very low in the cochlea as well as in the central nervous system [Mikawa et al., 2009].

In the kidney, PC(16:0/18:2) was localized in the medulla renalis [Sugiura and Setou, 2009], which is composed of the proximal tubule, the loop of Henle, distal tubule, and collecting duct. These regions are well known to contribute to K^+ cycling in the kidney [Lang et al., 2007]. In this study, PC(16:0/18:2) was observed primarily in the spiral ligament. The spiral ligament is composed of five types of fibrocytes connected by gap junctions, and also expresses ion channels and transporters for K^+ cycling [Lang et al., 2007]. The localization of PC(16:0/18:2) in the spiral ligament is of interest in light of the resemblance between the lateral wall of the cochlear duct and the kidney in ion cycling systems. Additionally, PC(16:0/18:1) was localized in the stria vascularis at the lateral wall of the cochlear duct. The clear differential distribution in the lateral wall of the cochlear duct seems to suggest a functional difference between PC(16:0/18:2) and PC(16:0/18:1). PC(16:0/16:1) was highly localized in the organ of Corti. This PC has not been identified in the central nervous system [Mikawa et al., 2009] or the kidney [Sugiura and Setou, 2009]. The development of methods to retain the fine structure of the organ of Corti will lead us to differentiate the sensory cells from the supporting cells in reconstructive images.

IMS can be used to analyze the distribution and detailed structures of the fatty acids in phospholipids in tissue sections. To date, many PC species have been located in a number of organs [Hayasaka et al., 2009; Zaima et al., 2009]. However, the roles of these PC species remain to be elucidated. Studying the distribution of PC species at different developmental stages and in pathological animal models, such as age-related, noise-induced, and oxidant stress models, will assist in revealing these roles in the future.

In conclusion, we have demonstrated the localization of five PC species in the cochlea using mass microscopy.

PC(16:0/16:0) was observed in the cochlear nerve in the modiolus and the neurons in the osseous spiral lamina, PC(16:0/18:1) in the organ of Corti and the stria vascularis, and PC(16:0/18:2) in the spiral ligament. The localization of PC(16:0/16:1) in the organ of Corti is unique compared to the central nervous system and the kidney. The differing distributions of the PC species may be related to the cellular architecture of each cochlear region.

Acknowledgments

We are grateful to Dr. T. Yamatodani, Dr. M. Arai, and Dr. Y. Hashimoto for their technical support with the guinea pig experiment, and to Dr. K.H. Iwasa for providing many valuable insights into the cochlear structure and function. This work was supported by a Grant-in-Aid for WAKATE-S from the Japan Society for the Promotion of Science (to M.S.) and SENTAN grants from the Japan Science and Technology Agency (to M.S.) and the Acute Profound Deafness Research Committee of the Ministry of Health, Labor and Welfare, Tokyo, Japan (to K.M.).

References

Adato A, Lefevre G, Delprat B, Michel V, Michalski N, Chardenoux S, Weil D, El-Amraoui A, Petit C: Usherin, the defective protein in Usher syndrome type IIA, is likely to be a component of interstereocilia ankle links in the inner ear sensory cells. Hum Mol Genet 2005;14:3921–3932.

Ashmore J, Gale J: The cochlea. Curr Biol 2000; 10:R325–R327.

Benzi G, Pastoris O, Marzatico F, Villa RF: Cerebral enzyme antioxidant system. Influence of aging and phosphatidylcholine. J Cereb Blood Flow Metab 1989;9:373–380.

Harada T, Yuba-Kubo A, Sugiura Y, Zaima N, Hayasaka T, Goto-Inoue N, Wakui M, Suematsu M, Takeshita K, Ogawa K, Yoshida Y, Setou M: Visualization of volatile substances in different organelles with an atmospheric-pressure mass microscope. Anal Chem 2009; 81:9153–9157.

Hayasaka T, Goto-Inoue N, Sugiura Y, Zaima N, Nakanishi H, Ohishi K, Nakanishi S, Naito T, Taguchi R, Setou M: Matrix-assisted laser desorption/ionization quadrupole ion trap time-of-flight (MALDI-QIT-TOF)-based imaging mass spectrometry reveals a layered distribution of phospholipid molecular species in the mouse retina. Rapid Commun Mass Spectrom 2008;22:3415–3426.

Hayasaka T, Goto-Inoue N, Zaima N, Kimura Y, Setou M: Organ-specific distributions of lysophosphatidylcholine and triacylglycerol in mouse embryo. Lipids 2009;44:837–848.

Hosokawa S, Mizuta K, Nakanishi H, Hashimoto Y, Arai M, Mineta H, Shindo S, Ikezono T: Ultrastructural localization of cochlin in the rat cochlear duct. Audiol Neurootol 2009;15: 247–253.

Hsu FF, Turk J: Electrospray ionization/tandem quadrupole mass spectrometric studies on phosphatidylcholines: the fragmentation processes. J Am Soc Mass Spectrom 2003;14: 352–363.

Kathiresan T, Harvey M, Orchard S, Sakai Y, Sokolowski B: A protein interaction network for the large conductance Ca(2+)-activated K(+) channel in the mouse cochlea. Mol Cell Proteomics 2009;8:1972–1987.

Kimura Y, Tsutsumi K, Sugiura Y, Setou M: Medical molecular morphology with imaging mass spectrometry. Med Mol Morphol 2009;42:133–137.

Kuksis A, Marai L: Determination of the complete structure of natural lecithins. Lipids 1967;2:217–224.

Lang F, Vallon V, Knipper M, Wangemann P: Functional significance of channels and transporters expressed in the inner ear and kidney. Am J Physiol Cell Physiol 2007; 293:C1187–C1208.

Lechene C, Hillion F, McMahon G, Benson D, Kleinfeld AM, Kampf JP, Distel D, Luyten Y, Bonventre J, Hentschel D, Park KM, Ito S, Schwartz M, Benichou G, Slodzian G: High-resolution quantitative imaging of mammalian and bacterial cells using stable isotope mass spectrometry. J Biol 2006;5:20.

McFadden SL, Ding D, Reaume AG, Flood DG, Salvi RJ: Age-related cochlear hair cell loss is enhanced in mice lacking copper/zinc superoxide dismutase. Neurobiol Aging 1999;20: 1–8.

Mikawa S, Suzuki M, Fujimoto C, Sato K: Imaging of phosphatidylcholines in the adult rat brain using MALDI-TOF MS. Neurosci Lett 2009;451:45–49.

Mizuta K, Saito A, Watanabe T, Nagura M, Arakawa M, Shimizu F, Hoshino T: Ultrastructural localization of megalin in the rat cochlear duct. Hear Res 1999;129:83–91.

Niedzielski AS, Schacht J: Phospholipid metabolism in the cochlea: differences between base and apex. Hear Res 1991;57:107–112.

Ogawa K, Schacht J: G-proteins coupled to phosphoinositide hydrolysis in the cochlear and vestibular sensory epithelia of the rat are insensitive to cholera and pertussis toxins. Hear Res 1994;74:197–203.

Seidman MD, Khan MJ, Tang WX, Quirk WS: Influence of lecithin on mitochondrial DNA and age-related hearing loss. Otolaryngol Head Neck Surg 2002;127:138–144.

Shimma S, Sugiura Y, Hayasaka T, Zaima N, Matsumoto M, Setou M: Mass imaging and identification of biomolecules with MALDI-QIT-TOF-based system. Anal Chem 2008; 80:878–885.

Sugiura Y, Konishi Y, Zaima N, Kajihara S, Nakanishi H, Taguchi R, Setou M: Visualization of the cell-selective distribution of PUFA-containing phosphatidylcholines in mouse brain by imaging mass spectrometry. J Lipid Res 2009;50:1776–1788.

Sugiura Y, Setou M: Selective imaging of positively charged polar and nonpolar lipids by optimizing matrix solution composition. Rapid Commun Mass Spectrom 2009;23: 3269–3278.

Sugiura Y, Setou M: Imaging mass spectrometry for visualization of drug and endogenous metabolite distribution: toward in situ pharmacometabolomes. J Neuroimmune Pharmacol 2010;5:31–43.

Swan EE, Peppi M, Chen Z, Green KM, Evans JE, McKenna MJ, Mescher MJ, Kujawa SG, Sewell WF: Proteomics analysis of perilymph and cerebrospinal fluid in mouse. Laryngoscope 2009;119:953–958.

Wangemann P: Supporting sensory transduction: cochlear fluid homeostasis and the endocochlear potential. J Physiol 2006;576:11–21.

Wangemann P, Schacht J: Homeostatic mechanisms in the cochlea; in Dallos P, Popper AN, Fay RR (eds): The Cochlea. New York, Springer, 1996, pp 130–185.

Yamasoba T, Nuttall AL, Harris C, Raphael Y, Miller JM: Role of glutathione in protection against noise-induced hearing loss. Brain Res 1998;784:82–90.

Yao I, Sugiura Y, Matsumoto M, Setou M: In situ proteomics with imaging mass spectrometry and principal component analysis in the Scrapper-knockout mouse brain. Proteomics 2008;8:3692–3701.

Zaima N, Hayasaka T, Goto-Inoue N, Setou M: Imaging of metabolites by MALDI mass spectrometry. J Oleo Sci 2009;58:415–419.

Cao et al. BMC Neuroscience 2010, 11:115
http://www.biomedcentral.com/1471-2202/11/115

BMC Neuroscience

RESEARCH ARTICLE Open Access

Delayed neuronal cell death in brainstem after transient brainstem ischemia in gerbils

Fang Cao[1], Ryuji Hata[1*], Pengxiang Zhu[1], Shoichiro Takeda[2], Tadashi Yoshida[2], Nobuhiro Hakuba[2], Masahiro Sakanaka[1], Kiyofumi Gyo[2]

Abstract

Background: Because of the lack of reproducible brainstem ischemia models in rodents, the temporal profile of ischemic lesions in the brainstem after transient brainstem ischemia has not been evaluated intensively. Previously, we produced a reproducible brainstem ischemia model of Mongolian gerbils. Here, we showed the temporal profile of ischemic lesions after transient brainstem ischemia.

Results: Brainstem ischemia was produced by occlusion of the bilateral vertebral arteries just before their entry into the transverse foramina of the cervical vertebrae of Mongolian gerbils. Animals were subjected to brainstem ischemia for 15 min, and then reperfused for 0 d (just after ischemia), 1 d, 3 d and 7 d (n = 4 in each group). Sham-operated animals (n = 4) were used as control. After deep anesthesia, the gerbils were perfused with fixative for immunohistochemical investigation. Ischemic lesions were detected by immunostaining for microtubule-associated protein 2 (MAP2). Just after 15-min brainstem ischemia, ischemic lesions were detected in the lateral vestibular nucleus and the ventral part of the spinal trigeminal nucleus, and these ischemic lesions disappeared one day after reperfusion in all animals examined. However, 3 days and 7 days after reperfusion, ischemic lesions appeared again and clusters of ionized calcium-binding adapter molecule-1(IBA-1)-positive cells were detected in the same areas in all animals.

Conclusion: These results suggest that delayed neuronal cell death took place in the brainstem after transient brainstem ischemia in gerbils.

Background

In the central nervous system, certain areas are selectively damaged even after a brief ischemic insult, and this topographical heterogeneity is known as "selective vulnerability of the brain". Hippocampal CA1 and neocortical III, V, and VI are extremely vulnerable to ischemia and hypoxia [1]. The mechanism responsible for this vulnerability is of particular importance to establish therapeutic procedures, because elucidation of the mechanism may lead to the development of novel therapy to ameliorate ischemic damage.

Pathologic aspects and the topographic distribution of ischemic lesions after transient ischemia have been extensively studied in the rodent forebrain [2,3]. However, little is known about the distribution of ischemic lesions after transient brainstem ischemia because of the lack of reproducible brainstem ischemia models in rodents. Previously, we established a brainstem ischemia model in gerbils by occlusion of the bilateral vertebral arteries, and demonstrated selective vulnerability after permanent brainstem ischemia [4]. This gerbil model has the following advantages: (1) it produces brainstem ischemia without intracranial injury, (2) it produces severe, reproducible brainstem ischemia, and (3) it allows reperfusion.

In the present study, using this animal model, we investigated the temporal profile of ischemic lesions in the brainstem after transient brainstem ischemia in gerbils. We demonstrated ischemic lesions by immunostaining for microtubule-associated protein 2 (MAP2) in the lateral vestibular nucleus and the ventral part of the spinal trigeminal nucleus three days after transient brainstem ischemia, while these ischemic lesions were not found one day after ischemia. This delayed neuronal

* Correspondence: hata@m.ehime-u.ac.jp
[1]Department of Functional Histology, Ehime University Graduate School of Medicine, Shitsukawa, Toon, Ehime 791-0295, Japan
Full list of author information is available at the end of the article

damage in the brainstem is reminiscent of the delayed neuronal cell death in the hippocampus after transient forebrain ischemia [5].

Methods

Animals and surgical procedure

Adult 12-16 week-old male Mongolian gerbils, weighing 60-80 g, were used in this study. All experiments were approved by the Ethics Committee of Ehime University Graduate School of Medicine and were conducted according to the Guidelines for Animal Experimentation at Ehime University Graduate School of Medicine. The gerbils were housed in an animal room with a temperature of 21 to 23°C and a 12-hour light/dark cycle (light on: 7 a.m. to 7 p.m.). The animals were allowed free access to food and water until the end of the experiment.

The gerbils were randomly divided into four groups, which were subjected to brainstem ischemia for 15 min and reperfused for 0 d (just after ischemia), 1 d, 3 d and 7 d (n = 4 in each group). Sham-operated animals (n = 4) were used as control. Animals were anesthetized with 1% halothane in 70% N_2O and 30% O_2. Anesthetized animals were orotracheally intubated with a ventilation tube. To facilitate access to the vertebral arteries, animals were placed in the supine position on a table tilted at approximately 30° to the horizontal. An anterior midline cervical incision was made, and the musculi longus colli were dissected to expose the vertebral arteries just before their entry into the transverse foramina of the cervical vertebrae. Both vertebral arteries were looped with 4-0 silk sutures. Then, the suture around each vertebral artery was pulled by a 5-g weight to occlude the circulation for 15 min. Consequently, apnea was observed within 1 min after occlusion, and subsequent convulsions were observed in all four limbs for about 1 min. After convulsions had ceased, all animals became unresponsive and lost their corneal reflex. Mechanical ventilation was initiated immediately after apnea was elicited during ischemia. The tidal volume was set to 1 ml and the rate was set to 70 breaths per minute. After 15 min of ischemia, the sutures were cut and removed to allow recirculation, which was confirmed by visual observation through an operating microscope. Within 10 min after reperfusion, spontaneous breathing reappeared and mechanical ventilation was ceased within 15 min after reperfusion.

Rectal temperature was maintained between 36.5 and 37.0°C by a heating lamp and a heating pad connected to a thermistor (ATB-1100, Nihon Koden, Tokyo, Japan) during surgery and until 1 h after reperfusion. After resuscitation, the animals were maintained in an air-conditioned room at about 22°C.

Histological procedures

After deep anesthesia with a lethal dose of sodium pentobarbital (0.1 g/kg), the gerbils were perfused with 4% paraformaldehyde in 0.1 M phosphate buffer (pH 7.4) and the brain was dissected out. After fixation with the same fixative for overnight the brain was dehydrated and embedded in paraffin. To investigate the temporal profile of ischemic lesions in the brainstem, we performed immunostaining for MAP2, IBA-1 and GFAP at the level of the lateral vestibular nucleus in the brainstem (5.5 mm caudal to the bregma) since this area has been reported to be most vulnerable to ischemia [4]. Coronal 5-μm-thick sections were examined by immunostaining for microtubule-associated protein 2 (MAP2), IBA-1 and glial fibrillary acidic protein (GFAP). Sections were immunostained using a Vectastain ABC Elite Kit (Vector Laboratories; Burlingame, Calif) with polyclonal anti-MAP2 (donated by Dr. Niinobe, Osaka University), polyclonal anti-IBA-1 (019-19741, Wako, Osaka, Japan) or monoclonal anti-GFAP (G9369, Sigma, St. Louis, USA) antibodies. Endogenous peroxidase in deparaffinized tissue sections was blocked for 10 minutes with 3% H_2O_2 in deionized water, followed by blocking with 10% goat serum diluted in 0.2% Tween-20 in phosphate buffered saline at room temperature for 1 hour. The tissues were then incubated with primary antibody (anti-MAP2, 1:1000; anti-IBA-1, 1:500; anti-GFAP, 1:500) at 4°C overnight. Tissue sections were washed and incubated with secondary antibody (1:1000) for 1 hour at room temperature. After washing, sections were incubated with ABC complex for 30 minutes at room temperature, and then stained with the chromogenic substrate 3, 3-diaminobenzidine tetrahydrochloride (DAB) and H_2O_2, until optimal staining was obtained.

Measurement of ischemic lesions

MAP2-stained sections were analyzed and images were viewed using a microscope (ECLIPSE E800, Nikon, Tokyo, Japan). The ischemic lesions detected by the loss of immunoreaction for MAP2 were measured and quantification was performed on images using ImageJ software (National Institutes of Health, Bethesda, MD).

Statistics

All values are given as mean ± SD. Statistical analysis was performed with the Statistical Package for the Social Sciences, release 15 (SPSS ver. 15). Differences were analyzed using one-way ANOVA followed by Bonferroni's multiple comparison test. A p value of less than 0.05 was considered to indicate statistical significance.

Results

Immunohistochemical investigation

Four gerbils each were used for the reperfusion periods of 0, 1 d, and 3 d. As for the reperfusion period of 7 d, we evaluated three animals because one animal died of respiratory failure 5 days after ischemia. Sham-operated animals (n = 4) were used as control. Loss of immunoreaction for MAP2 in neuropils, nerve cell bodies, and dendrites was used as the criterion for the presence of ischemic lesions. The findings were compared with those in sham-operated controls. Each brain section was examined by two investigators; and whenever there was any uncertainty, a third investigator examined the specimen without any prior information.

Just after brainstem ischemia

Ischemic lesions detected by immunostaining for MAP2 were found in the lateral vestibular nucleus (LVe; blue arrows in Figure 1B) and the ventral part of the spinal trigeminal nucleus (Sp5; red arrows in Figure 1B) in all 4 animals (100%). Higher magnification photomicrographs of ischemic lesions showed loss of immunoreaction for MAP2 in neuropils and nerve cell bodies in LVe (blue arrows in Figure 2B) and the ventral part of Sp5 (red arrows in Figure 3B). Compared with sham-operated controls, there was no change in IBA-1 (a marker of microglia and monocytic lineage) and GFAP (a marker of astrocytes) expression (Figure 1G and 1L).

One day after brainstem ischemia

No ischemic lesion was detected by MAP2 staining (Figure 1C). Furthermore, there was no change in IBA-1 and GFAP expression, compared with that in sham-operated controls (Figure 1H and 1M).

Three days after brainstem ischemia

Ischemic lesions in LVe (blue arrows in Figures 1D and 2D) and the ventral part of Sp5 (red arrows in Figures 1D and 3D) appeared again in all 4 animals (100%). Compared with the ischemic lesions just after brainstem ischemia, ischemic lesions in LV expanded ventrally to include the spinal vestibular nucleus (SpVe) in 2 out of 4 animals (50%). De novo ischemic lesions were detected in the dorsal part of Sp5 (blue arrowheads in Figures 1D and 3D) and ventral cochlear nucleus (VC) (red arrowheads in Figures1D and 4D) in 2 out of 4 animals (50%).

In addition, IBA-1 immunoreactivity was markedly up-regulated in the central part of the ischemic lesions where MAP2 immunostaining was lost. Up-regulation of IBA-1 immunoreactivity was detected in LVe (blue arrows in Figures 1I and 2I) and the ventral part of Sp5 (red arrows in Figures 1I and 3I) in 3 out of 4 animals (75%). Up-regulation of IBA-1 immunoreactivity was also detected in the dorsal part of Sp5 (blue arrowheads in Figures 1I and 3I) and ventral cochlear nucleus (VC) (red arrowheads in Figures 1I and 4I) in 2 out of 4 animals (50%). Higher magnification photomicrographs demonstrated strongly IBA-1-positive cells in these areas. These IBA-1-positive cells displayed an amoeboid shape including only small perisomal lamellopodial expansions or a few unbranched processes. They were morphologically easily distinguishable from ramified microglial cells, which were recognized by their thick processes and large cell bodies.

Furthermore, immunoreactivity for GFAP disappeared in ischemic lesions where immunostaining for MAP2 was lost, whereas immunoreactivity for GFAP increased in the neighboring areas around ischemic lesions. A reduction of GFAP staining was detected in LVe (blue arrows in Figures 1N and 2N) and the ventral part of Sp5 (red arrows in Figures 1N and 3N) in 3 out of 4 animals (75%). A reduction of GFAP staining was also detected in the dorsal part of Sp5 (blue arrowheads in Figures 1N and 3N) and the ventral cochlear nucleus (VC) (red arrowheads in Figures 1N and 4N) in 2 out of 4 animals (50%). Higher magnification photomicrographs showed that GFAP-positive astrocytes were not observed in ischemic lesions where immunostaining for MAP2 was lost. Reactive astrocytes with thick, long GFAP-positive processes were distributed around ischemic lesions.

Seven days after brainstem ischemia

Ischemic lesions detected by immunostaining for MAP2 expanded further (Figure 5A-D). Ischemic lesions in LVe (blue arrows in Figures 1E and 2E) and the ventral part of Sp5 (red arrows in Figures 1E and 3E) appeared in all 3 animals (100%). Ischemic lesions were also detected in the dorsal part of Sp5 (blue arrowheads in Figures 1E and 3E) and the ventral cochlear nucleus (VC) (red arrowheads in Figures 1E and 4E) in 1 out of 3 animals (33%).

IBA-1 immunoreactivity was markedly up-regulated in ischemic lesions where MAP2 immunostaining was lost. Compared with the profile of IBA-1 staining three days after brainstem ischemia, strongly IBA-1-positive cells with an amoeboid shape were distributed more peripherally in ischemic lesions as well as in the center of ischemic lesions. Up-regulation of IBA-1 immunoreactivity was detected in LVe (blue arrows in Figures 1J and 2J) and the ventral part of Sp5 (red arrows in Figures 1J and 3J) in all three animals (100%). Up-regulation of IBA-1 immunoreactivity was also detected in the dorsal part of Sp5 (blue arrowheads in Figures 1J and 3J) and ventral cochlear nucleus (VC) (red arrowheads in Figures 1J and 4J) in one out of three animals (33%).

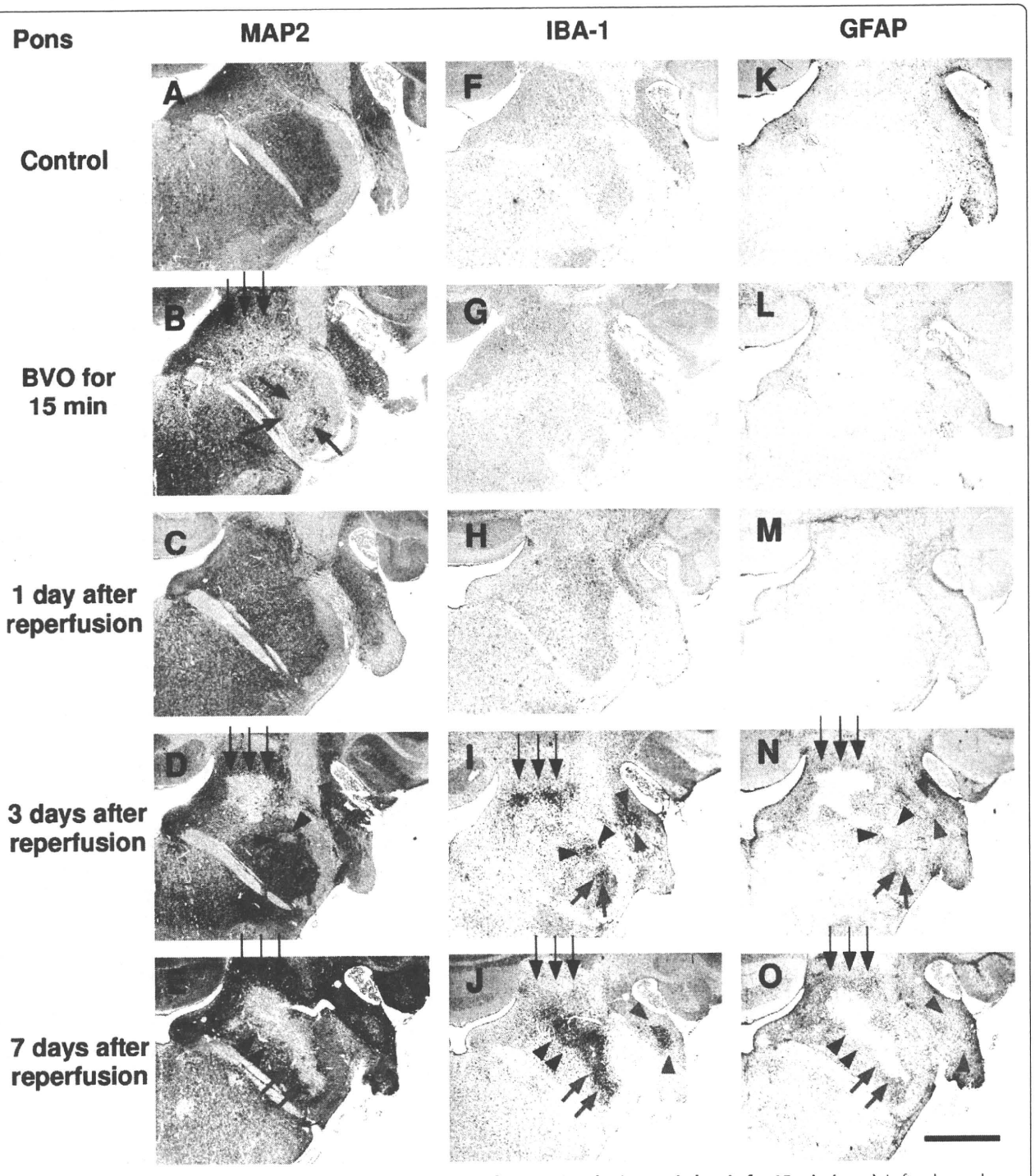

Figure 1 Representative photomicrographs of immunostaining after transient brainstem ischemia for 15 min (pons). Left column shows immunoreactivity for MAP2 (A-E); middle column shows immunoreactivity for IBA-1 (F-J); right column shows immunoreactivity for GFAP (K-O). Ischemic lesions with loss of MAP2 staining were detected in the lateral vestibular nucleus (LVe: B; blue arrows) and the ventral part of the spinal trigeminal nucleus (Sp5: B; red arrows) after bilateral vertebral artery occlusion (BVO) for 15 min. These ischemic lesions had disappeared at 1 day after reperfusion (C). At 3 days and 7 days after reperfusion, ischemic lesions appeared again and expanded further (D and E; blue and red arrows). New ischemic lesions were detected in the dorsal part of Sp5 (D and E; blue arrowheads) and ventral cochlear nucleus (VC) (D and E; red arrowheads). At the same time, clusters of amoeboid microglia/macrophages were detected in the same areas (I and J; blue and red arrows/arrowheads). At 3 days and 7 days after reperfusion, immunoreactivity for GFAP was lost in the ischemic lesions, and increased immunoreactivity for GFAP was detected around ischemic lesions (N and O; blue and red arrows/arrowheads). Scale bar = 1 mm.

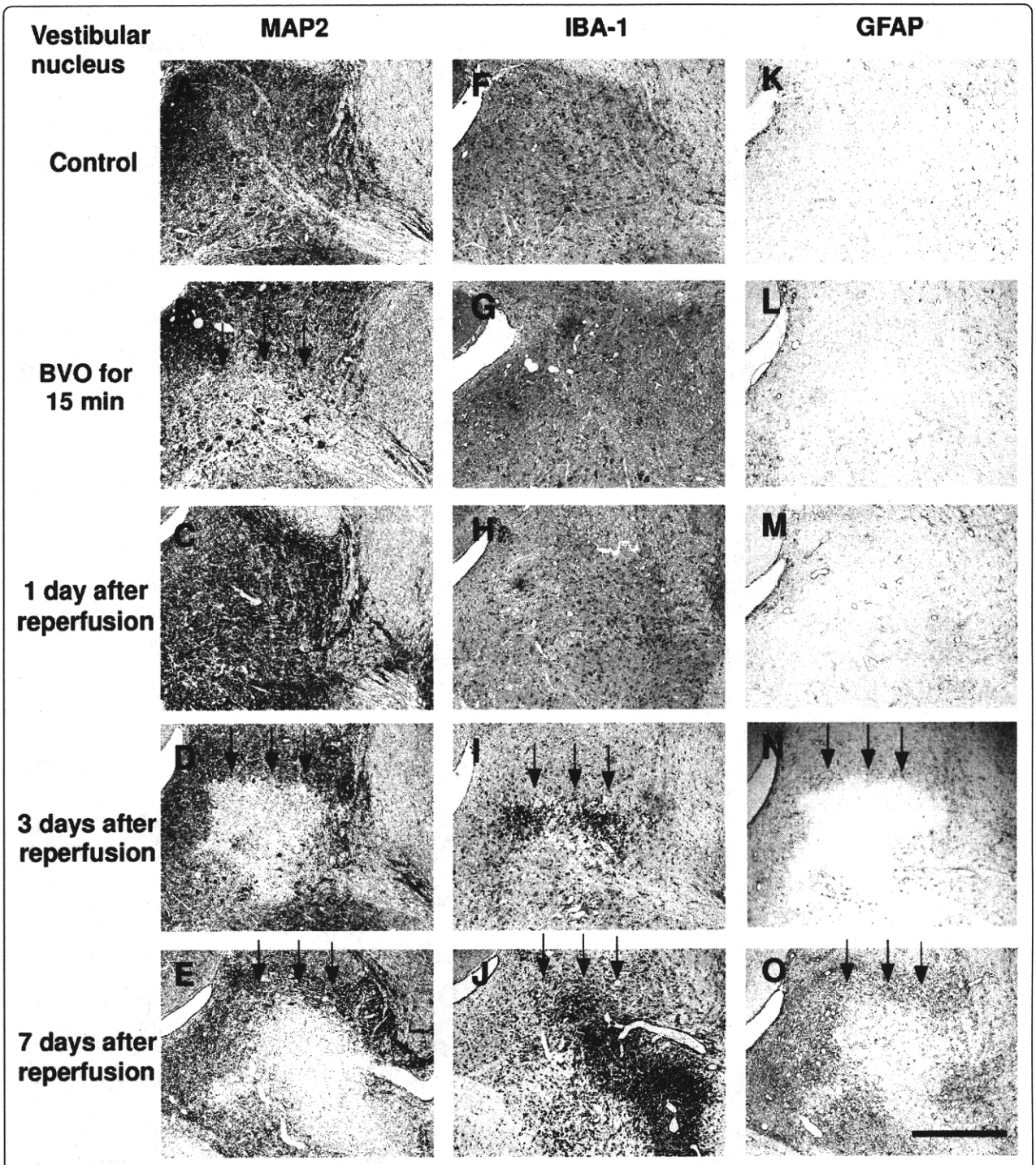

Figure 2 Representative photomicrographs of immunostaining after transient brainstem ischemia for 15 min (vestibular nucleus). Left column shows immunoreactivity for MAP2 (A-E); middle column shows immunoreactivity for IBA-1 (F-J); right column shows immunoreactivity for GFAP (K-O). Ischemic lesions with loss of immunoreactivity for MAP2 were seen in the lateral vestibular nucleus after bilateral vertebral artery occlusion (BVO) for 15 min (B; blue arrows), and these lesions had disappeared at 1 day after reperfusion (C). However, ischemic lesions had reappeared and expanded further at 3 days and 7 days after reperfusion (D and E; blue arrows). Clusters of IBA-1-positive amoeboid microglia/macrophages (I and J; blue arrows) and loss of expression of GFAP (N and O; blue arrows) were detected in the same areas where MAP2 expression was markedly lost at 3 days and 7 days after reperfusion. Increased immunoreactivity for GFAP (N and O; blue arrows) was also detected around ischemic lesions at 3 days and 7 days after reperfusion. Scale bars = 0.5 mm.

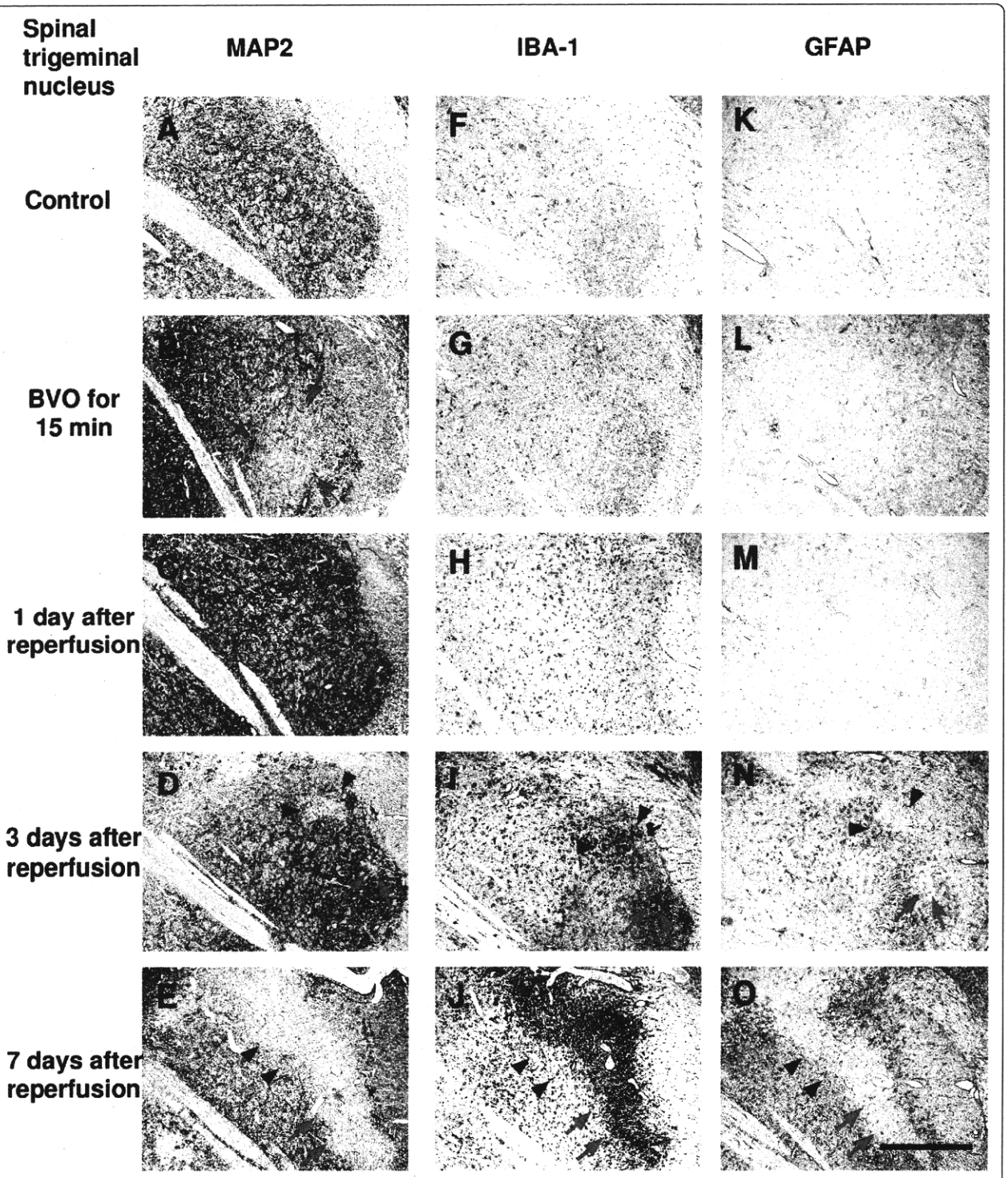

Figure 3 Representative photomicrographs of immunostaining after transient brainstem ischemia for 15 min (spinal trigeminal nucleus). Left column shows immunoreactivity for MAP2 (A-E); middle column shows immunoreactivity for IBA-1 (F-J); right column shows immunoreactivity for GFAP (K-O). Ischemic lesions with loss of immunoreactivity for MAP2 were seen in the ventral part of Sp5 after bilateral vertebral artery occlusion (BVO) for 15 min (B; red arrows), and these lesions had disappeared at 1 day after reperfusion (C). However, ischemic lesions had reappeared and expanded further (D and E; red arrows) and new ischemic lesions were detected in the dorsal part of Sp5 (D and E; blue arrowheads) at 3 days and 7 days after reperfusion. Clusters of IBA-1-positive amoeboid microglia/macrophages (I and J; red arrows and blue arrowheads) and loss of GFAP expression (N and O; red arrows and blue arrowheads) were detected in the same areas where MAP2 expression was lost at 3 days and 7 days after reperfusion. Increased immunoreactivity for GFAP (N and O; red arrows and blue arrowheads) was also detected around ischemic lesions at 3 days and 7 days after reperfusion. Scale bars = 0.5 mm.

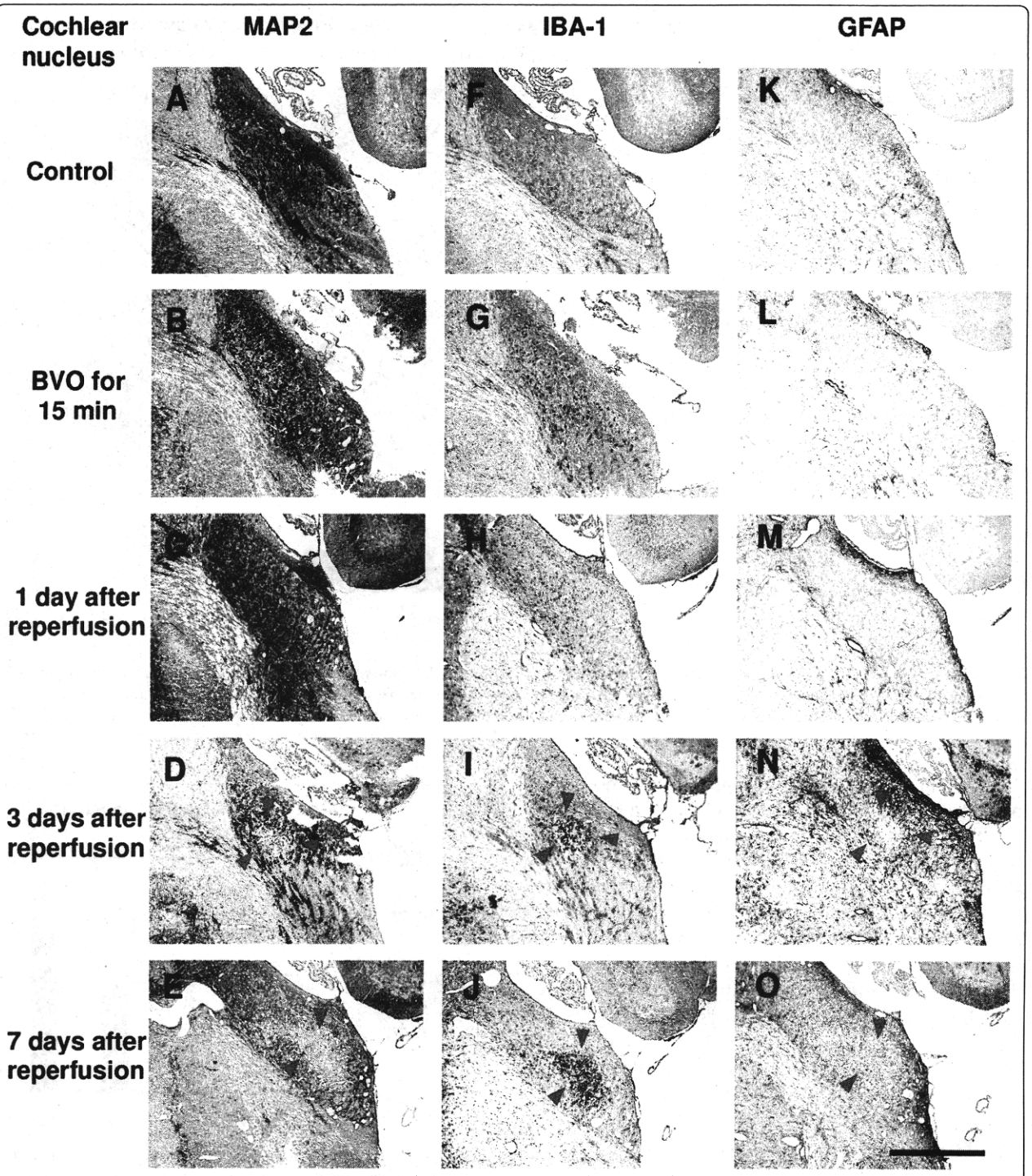

Figure 4 Representative photomicrographs of immunostaining after transient brainstem ischemia for 15 min (cochlear nucleus). Left column shows immunoreactivity for MAP2 (A-E); middle column shows immunoreactivity for IBA-1 (F-J); right column shows immunoreactivity for GFAP (K-O). Ischemic lesions with loss of immunoreactivity for MAP2 were seen in the ventral cochlear nucleus (VC) at 3 days and 7 days after reperfusion (D and E; red arrowheads). Clusters of IBA-1-positive amoeboid microglia/macrophages (I and J; red arrowheads) and loss of GFAP expression (N and O; red arrowheads) were detected in the same areas where MAP2 expression was lost at 3 days and 7 days after reperfusion. Increased immunoreactivity for GFAP (N and O; red arrowheads) was also detected around ischemic lesions at 3 days and 7 days after reperfusion. Scale bars = 0.5 mm.

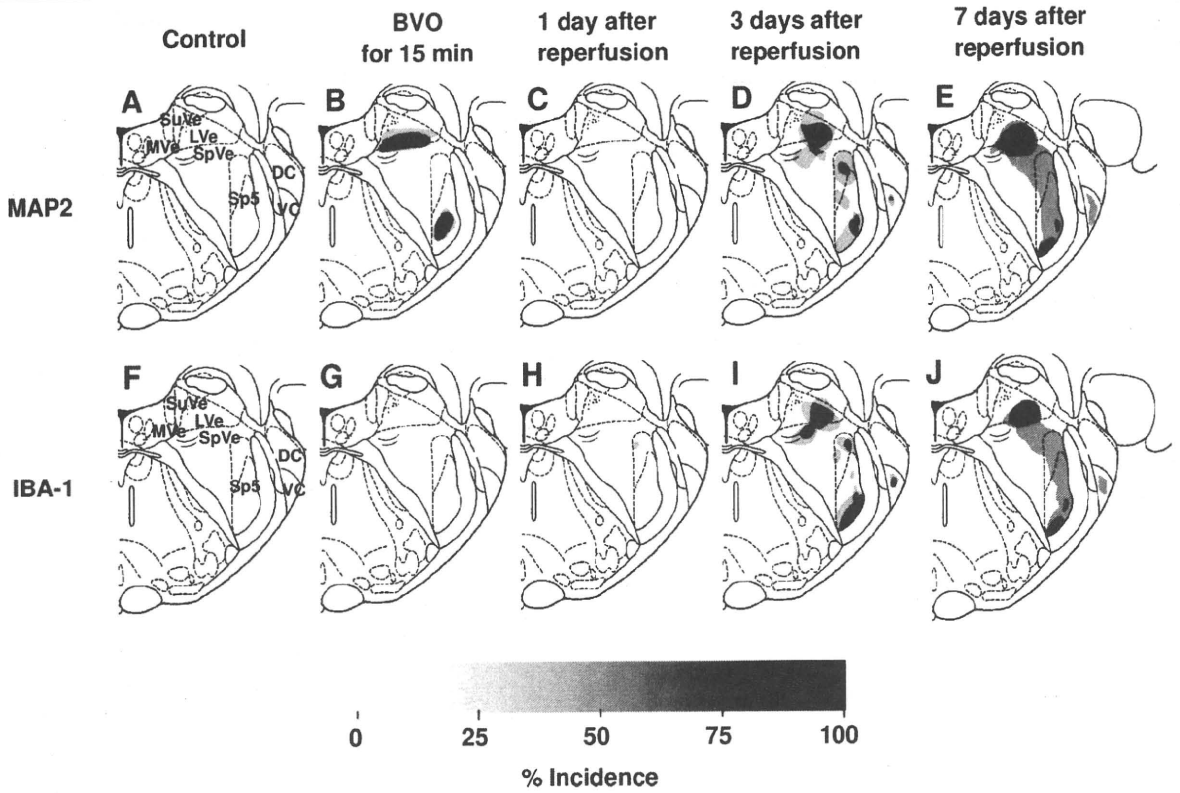

Figure 5 Incidence maps of immunoreactivity for MAP2 (decrease) and IBA-1(increase) in coronal gerbil brain sections at various times after transient brainstem ischemia for 15 min (at level of pons [5.5 mm caudal to bregma]). Areas of altered immunoreactivity were outlined in all animals examined and superimposed to represent the incidence map (%). For details, see text.

GFAP immunoreactivity disappeared in the central part of ischemic lesions where MAP2 immunostaining was lost. Immunoreactivity for GFAP increased in the periphery of ischemic lesions as well as the neighboring areas around ischemic lesions. These results suggested that reactive astrocytes proliferated in the neighboring areas around ischemic lesions and migrated into the ischemic lesions. A reduction of GFAP staining was detected in LVe (blue arrows in Figures 1O and 2O) and the ventral part of Sp5 (red arrows in Figures 1O and 3O) in all 3 animals (100%). A reduction of GFAP staining was also detected in the dorsal part of Sp5 (blue arrowheads in Figures 1O and 3O) and the ventral cochlear nucleus (VC) (red arrowheads in Figures 1O and 4O) in 1 out of 3 animals (33%).

Temporal profile of ischemic lesions

The total area of ischemic lesions detected by MAP2 staining in each animal was calculated and summarized in Figure 6. Just after brainstem ischemia for 15 min, the total area of ischemic lesions was 0.33 ± 0.041 [Mean ± SD] (mm^2). Although ischemic lesions disappeared one day after brainstem ischemia, evolution of ischemic lesions was detected 3 and 7 days after

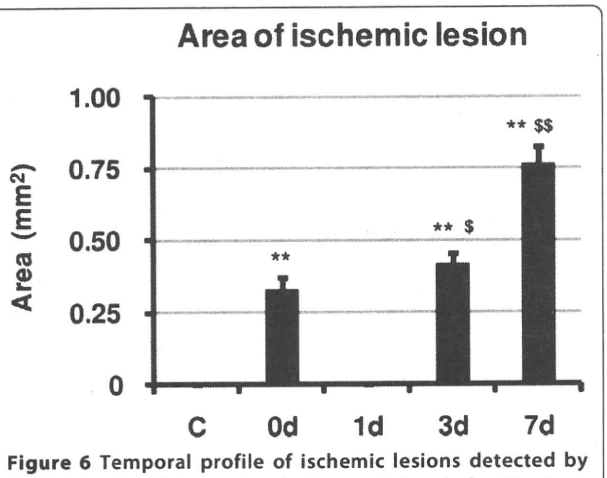

Figure 6 Temporal profile of ischemic lesions detected by MAP2 staining after transient brainstem ischemia for 15 min. The area of ischemic lesions detected by MAP2 staining in each animal was calculated. For details, see text. C: control, 0 d: just after brainstem ischemia for 15 min, 1 d, 3 d and 7 d: 1, 3 and 7 days after transient brainstem ischemia for 15 min, respectively. All values are given as mean ± SD. Differences were analyzed using one-way ANOVA followed by Bonferroni's multiple comparison test. A p value of less than 0.05 was considered to indicate statistical significance. ** and $$ indicate significant ($p < 0.01$) difference vs. C and 0 d, respectively. $ indicates significant ($p < 0.05$) difference vs. 0 d.

transient brainstem ischemia (0.42 ± 0.034 and 0.76 ± 0.064, respectively).

Discussion

Detection of morphological damage in early cerebral ischemia is difficult with conventional histological procedures including triphenyltetrazolium chloride and hematoxylin-eosin staining. With these conventional methods, morphological evidence of neuronal death does not become apparent until 1 to 2 hours after the onset of cerebral ischemia. However, early ischemic lesions can now be detected by applying immunohistochemical methods, and a reduction in microtubule-associated protein 2 (MAP2) immunoreactivity has been found to be an early, sensitive marker of ischemic neuronal damage [6]. In our study, by using this method, we showed that the lateral vestibular nucleus (LVe) and the ventral part of the spinal trigeminal nucleus (vSp5) were particularly vulnerable to ischemia.

In the LVe, multipolar giant neurons (Deiter's neurons) were most vulnerable to ischemia. Vestibular neurons receive excitatory glutaminergic input from the vestibular nerve [7] and commissural excitatory afferents [8]. Immunohistochemical and in situ hybridization histochemical studies revealed the highest glutamate receptor 2 (GluR2) expression in giant Deiter's neurons of the lateral vestibular nucleus and the lowest expression in small neurons throughout the vestibular nuclei [9]. These reports suggest that Deiter's neurons receive excitatory input and have selective sensitivity to excitotoxicity. As an analogy to hippocampal neurons [10], we speculate that an ischemia-induced alteration of GluR2 expression in Deiter's neurons induced cell death. Although further investigations are required to clarify the mechanisms underlying this selective vulnerability and delayed neuronal damage, they may also be related to several other factors such as the degree of cerebral hypoperfusion after reperfusion [11], inhibition of protein synthesis [12], neutrophil infiltration following reperfusion [13], free radical production [14], dysfunction of the mitochondrial shuttle system [15] or apoptosis [16].

Furthermore, we showed that the ischemic lesions in LVe and vSp5 had disappeared one day after reperfusion, but appeared again three days after reperfusion and thereafter. The observed loss of immunoreaction for MAP2 may reflect cytoskeletal breakdown, because MAP2 is involved in maintaining the structural integrity of the neuronal cytoskeleton [17]. The ischemia-induced rapid elevation of intracellular Ca^{2+} concentration and subsequent activation of Ca^{2+}-dependent phosphatases (e.g., calcineurin) and proteases (e.g., calpains) can lead to dephosphorylation and proteolytic degradation of MAP2 [18,19]. Therefore, ischemia-induced loss of immunoreaction for MAP2 is considered to be a reliable marker of neurons that are already undergoing irreversible processes in cell death [20]. However, Kitagawa et al. showed that loss of MAP2 immunostaining preceded the development of overt neuronal loss in a gerbil model of transient forebrain ischemia [6]. Our results are also consistent with this notion that MAP2 immunostaining can be used as an indicator of still viable neurons that will undergo irreversible injury only at a later time point.

We also demonstrated clusters of IBA-1-expressing cells in the ischemic lesions where MAP2 staining was lost three days after ischemia and thereafter. The rat *Iba1* gene has been identified as a microglia-specific transcript [21]. The isolated *Iba1*clone was 0.8 kb, a rather small cDNA encoding a 17-kDa protein consisting of 147 amino acids. IBA-1 is an interferon-γ (IFN-γ)-inducible Ca^{2+}-binding EF-hand protein that is encoded within the HLA class III genomic region. Expression of IBA-1 is mostly limited to the monocyte/macrophage lineage, and is augmented by cytokines such as IFN-γ. It was assumed that IBA-1 is a novel molecule involved in inflammatory responses and allograft rejection, as well as activation of macrophages [22]. In the normal brain, IBA-1 is highly expressed in resident microglial cells, but is never expressed in neurons and astrocytes [22]. After ischemia, IBA-1 is also expressed in activated resident microglial cells and infiltrating hematogenous macrophages [23,24].

Resident microglial cells rapidly became activated after ischemia. They developed amoeboid or rounded cell bodies and migrated rapidly into the ischemic lesion. For example, IBA-1 expression was rapidly up-regulated in the gerbil hippocampal CA1 region at 30 min after transient forebrain ischemia for 5 min [25]. However, microglial cells did not proliferate rapidly. Denes et al. showed that resident microglial cells exhibited intense proliferation at 48 and 72 h after transient occlusion of the middle cerebral artery (MCA) in the mouse. Average microglial cell number in the ischemic lesion did not increase significantly up to 48 h after transient ischemia [26]. We also demonstrated that a significant increase in Iba-1-positive cells was not detected in the ischemic cortex of the rat until one day after permanent MCA occlusion (MCAO), while a significant decrease in Iba-1-positive cells was detected even 2 h after permanent MCAO[27]. Furthermore, infiltrating hematogenous macrophages do not appear in the brain within one day after ischemia [24]. In this study, we did not detect clusters of IBA-1-expressing cells (i.e. topical proliferation of microglial cells) within one day after ischemia. Clusters of IBA-1-expressing cells initially appeared in the core of the ischemic lesions three days after ischemia, and these IBA-1-positive cells exhibited round cell bodies

and possessed pseudopodia and thin filopodia-like processes, indicating a motile phagocytic phenotype. At seven days after ischemia, IBA-1-expressing cells with an amoeboid shape were distributed more peripherally in the ischemic lesions as well as in the core of the ischemic lesions. Based on their morphological features and the temporal profile of the distribution of IBA-1-positive cells in ischemic lesions, we speculated that these IBA-1-expressing cells were of hematopoietic origin, although we could not exclude the possibility that they were of resident microglial origin.

In addition, we showed that delayed progression of ischemic neural death took place in the brainstem. Although other morphological and biochemical investigations including electron microscopic study are required for further analysis, this delayed neuronal damage in the brainstem is reminiscent of the delayed neuronal death in the hippocampus after transient forebrain ischemia [5]. There is increasing evidence that microglial cells contribute to delayed neuronal death. Recruitment and activation of microglial cells gradually increase within the hippocampal CA1 area over 24 h after transient forebrain ischemia, before the degeneration of neurons [28]. Endangered neurons can release proinflammatory chemokines such as monocyte chemoattractant protein-1 (MCP-1/CCL2) and secondary lymphoid-tissue chemokine (SLC/CCL21). Expression of MCP-1 and SLC is increased in neurons after ischemia [29,30]. Subsequently, recruited and activated microglial cells produce inflammatory mediators, including interleukin-1β (IL-1β), tumor necrosis factor-α (TNF-α), and nitric oxide (NO), which contribute to delayed neuronal death [31]. Moreover, immunosuppressants, such as FK506, prevent microglial activation and neuronal damage after ischemia [32]. Consistent with these findings, our results also suggest that activated microglia/macrophages play a crucial role in this delayed neuronal cell death in the brainstem.

Conclusions

In conclusion, we evaluated the evolution of ischemic lesions in the brainstem after transient brainstem ischemia in gerbils. Using immunostaining for MAP2, ischemic lesions were detected in LVe and vSp5 in all four animals. These ischemic lesions disappeared one day after reperfusion, but appeared again three days after reperfusion and thereafter in all animals examined. In addition, clusters of activated microglia/macrophages were detected in these ischemic lesions three days after ischemia and thereafter. These results suggest that delayed neuronal cell death took place in the brainstem after transient brainstem ischemia in gerbils.

Abbreviations

SuVe: superior vestibular nucleus; MVe: medial vestibular nucleus; LVe: lateral vestibular nucleus; SpVe: spinal vestibular nucleus; DC: dorsal cochlear nucleus; VC: ventral cochlear nucleus; Sp5: spinal trigeminal nucleus; BVO: bilateral vertebral artery occlusion

Acknowledgements

This project was supported, in part, by grants from the Ministry of Education, Science, Sports and Culture of Japan. We are grateful for the secretarial assistance of Ms. K. Hiraoka.

Author details

[1]Department of Functional Histology, Ehime University Graduate School of Medicine, Shitsukawa, Toon, Ehime 791-0295, Japan. [2]Department of Otolaryngology, Ehime University Graduate School of Medicine, Shitsukawa, Toon-shi, Ehime 791-0295, Japan.

Authors' contributions

The original concept was by RH, MS and KG. Animal experiments were performed by ST and TY. Immunostaining was performed by FC and PZ. Evaluation of immunostaining was performed by FC, RH and NH. The manuscript was written and edited by FC and RH. All authors read and approved the final manuscript.

Competing interests

The authors declare that they have no competing interests.

Received: 21 March 2010 Accepted: 14 September 2010
Published: 14 September 2010

References

1. Auer RN, Benveniste H: *Hypoxia and related conditions* New York: Oxford University Press 1998.
2. Pulsinelli WA, Brierley JB, Plum F: **Temporal profile of neuronal damage in a model of transient forebrain ischemia.** *Ann Neurol* 1982, **11(5)**:491-498.
3. Smith ML, Auer RN, Siesjo BK: **The density and distribution of ischemic brain injury in the rat following 2-10 min of forebrain ischemia.** *Acta Neuropathol* 1984, **64(4)**:319-332.
4. Hata R, Matsumoto M, Hatakeyama T, Ohtsuki T, Handa N, Niinobe M, Mikoshiba K, Sakaki S, Nishimura T, Yanagihara T, *et al*: **Differential vulnerability in the hindbrain neurons and local cerebral blood flow during bilateral vertebral occlusion in gerbils.** *Neuroscience* 1993, **56(2)**:423-439.
5. Kirino T: **Delayed neuronal death in the gerbil hippocampus following ischemia.** *Brain Res* 1982, **239(1)**:57-69.
6. Kitagawa K, Matsumoto M, Niinobe M, Mikoshiba K, Hata R, Ueda H, Handa N, Fukunaga R, Isaka Y, Kimura K, *et al*: **Microtubule-associated protein 2 as a sensitive marker for cerebral ischemic damage-immunohistochemical investigation of dendritic damage.** *Neuroscience* 1989, **31(2)**:401-411.
7. Reichenberger I, Dieringer N: **Size-related colocalization of glycine and glutamate immunoreactivity in frog and rat vestibular afferents.** *J Comp Neurol* 1994, **349(4)**:603-614.
8. Doi K, Tsumoto T, Matsunaga T: **Actions of excitatory amino acid antagonists on synaptic inputs to the rat medial vestibular nucleus: an electrophysiological study in vitro.** *Exp Brain Res* 1990, **82(2)**:254-262.
9. Popper P, Rodrigo JP, Alvarez JC, Lopez I, Honrubia V: **Expression of the AMPA-selective receptor subunits in the vestibular nuclei of the chinchilla.** *Brain Res Mol Brain Res* 1997, **44(1)**:21-30.
10. Gorter JA, Petrozzino JJ, Aronica EM, Rosenbaum DM, Opitz T, Bennett MV, Connor JA, Zukin RS: **Global ischemia induces downregulation of Glur2 mRNA and increases AMPA receptor-mediated Ca2+ influx in hippocampal CA1 neurons of gerbil.** *J Neurosci* 1997, **17(16)**:6179-6188.
11. Hossmann KA: **Reperfusion of the brain after global ischemia: hemodynamic disturbances.** *Shock* 1997, **8(2)**:95-101.
12. Bodsch W, Takahashi K, Barbier A, Ophoff BG, Hossmann KA: **Cerebral protein synthesis and ischemia.** *Prog Brain Res* 1985, **63**:197-210.
13. Barone FC, Feuerstein GZ: **Inflammatory mediators and stroke: new opportunities for novel therapeutics.** *J Cereb Blood Flow Metab* 1999, **19(8)**:819-834.

14. Siesjo BK, Agardh CD, Bengtsson F: **Free radicals and brain damage.** *Cerebrovasc Brain Metab Rev* 1989, **1(3)**:165-211.
15. Abe K, Aoki M, Kawagoe J, Yoshida T, Hattori A, Kogure K, Itoyama Y: **Ischemic delayed neuronal death. A mitochondrial hypothesis.** *Stroke* 1995, **26(8)**:1478-1489.
16. Du C, Hu R, Csernansky CA, Hsu CY, Choi DW: **Very delayed infarction after mild focal cerebral ischemia: a role for apoptosis?** *J Cereb Blood Flow Metab.* 1996, **16(2)**:195-201.
17. Johnson GV, Jope RS: **The role of microtubule-associated protein 2 (MAP-2) in neuronal growth, plasticity, and degeneration.** *J Neurosci Res* 1992, **33(4)**:505-512.
18. Siman R, Noszek JC: **Excitatory amino acids activate calpain I and induce structural protein breakdown in vivo.** *Neuron* 1988, **1(4)**:279-287.
19. Halpain S, Greengard P: **Activation of NMDA receptors induces rapid dephosphorylation of the cytoskeletal protein MAP2.** *Neuron* 1990, **5(3)**:237-246.
20. Dawson DA, Hallenbeck JM: **Acute focal ischemia-induced alterations in MAP2 immunostaining: description of temporal changes and utilization as a marker for volumetric assessment of acute brain injury.** *J Cereb Blood Flow Metab* 1996, **16(1)**:170-174.
21. Imai Y, Ibata I, Ito D, Ohsawa K, Kohsaka S: **A novel gene iba1 in the major histocompatibility complex class III region encoding an EF hand protein expressed in a monocytic lineage.** *Biochem Biophys Res Commun* 1996, **224(3)**:855-862.
22. Imai Y, Kohsaka S: **Intracellular signaling in M-CSF-induced microglia activation: role of Iba1.** *Glia* 2002, **40(2)**:164-174.
23. Tanaka R, Komine-Kobayashi M, Mochizuki H, Yamada M, Furuya T, Migita M, Shimada T, Mizuno Y, Urabe T: **Migration of enhanced green fluorescent protein expressing bone marrow-derived microglia/macrophage into the mouse brain following permanent focal ischemia.** *Neuroscience* 2003, **117(3)**:531-539.
24. Schilling M, Besselmann M, Leonhard C, Mueller M, Ringelstein EB, Kiefer R: **Microglial activation precedes and predominates over macrophage infiltration in transient focal cerebral ischemia: a study in green fluorescent protein transgenic bone marrow chimeric mice.** *Exp Neurol* 2003, **183(1)**:25-33.
25. Hwang IK, Yoo KY, Kim DW, Choi SY, Kang TC, Kim YS, Won MH: **Ionized calcium-binding adapter molecule 1 immunoreactive cells change in the gerbil hippocampal CA1 region after ischemia/reperfusion.** *Neurochem Res* 2006, **31(7)**:957-965.
26. Denes A, Vidyasagar R, Feng J, Narvainen J, McColl BW, Kauppinen RA, Allan SM: **Proliferating resident microglia after focal cerebral ischaemia in mice.** *J Cereb Blood Flow Metab* 2007, **27(12)**:1941-1953.
27. Cao F, Hata R, Zhu P, Niinobe M, Sakanaka M: **Up-regulation of syntaxin1 in ischemic cortex after permanent focal ischemia in rats.** *Brain Res* 2009, **1272**:52-61.
28. Morioka T, Kalehua AN, Streit WJ: **The microglial reaction in the rat dorsal hippocampus following transient forebrain ischemia.** *J Cereb Blood Flow Metab* 1991, **11(6)**:966-973.
29. Che X, Ye W, Panga L, Wu DC, Yang GY: **Monocyte chemoattractant protein-1 expressed in neurons and astrocytes during focal ischemia in mice.** *Brain Res* 2001, **902(2)**:171-177.
30. Biber K, Sauter A, Brouwer N, Copray SC, Boddeke HW: **Ischemia-induced neuronal expression of the microglia attracting chemokine Secondary Lymphoid-tissue Chemokine (SLC).** *Glia* 2001, **34(2)**:121-133.
31. Wang HK, Park UJ, Kim SY, Lee JH, Kim SU, Gwag BJ, Lee YB: **Free radical production in CA1 neurons induces MIP-1alpha expression, microglia recruitment, and delayed neuronal death after transient forebrain ischemia.** *J Neurosci* 2008, **28(7)**:1721-1727.
32. Furuichi Y, Noto T, Li JY, Oku T, Ishiye M, Moriguchi A, Aramori I, Matsuoka N, Mutoh S, Yanagihara T: **Multiple modes of action of tacrolimus (FK506) for neuroprotective action on ischemic damage after transient focal cerebral ischemia in rats.** *Brain Res* 2004, **1014(1-2)**:120-130.

doi:10.1186/1471-2202-11-115
Cite this article as: Cao *et al.*: Delayed neuronal cell death in brainstem after transient brainstem ischemia in gerbils. *BMC Neuroscience* 2010 **11**:115.

Original Paper

Audiology Neurotology

Audiol Neurotol 2009;14:26–34
DOI: 10.1159/000151587

Received: January 9, 2008
Accepted after revision: May 14, 2008
Published online: August 27, 2008

Long-Term Prognosis of Steroid-Dependent Sensorineural Hearing Loss

Jin Kanzaki[a, b] Sho Kanzaki[a] Kaoru Ogawa[a]

[a]Department of Otolaryngology, Keio University, School of Medicine, Shinjuku, Tokyo, and [b]Department of Otolaryngology, International University of Health and Welfare, Atami, Japan

Key Words
Steroid-dependent sensorineural hearing loss · Long-term prognosis · Takayasu's arteritis

Abstract
We report on the long-term follow-up of 15 patients with steroid-dependent sensorineural hearing loss (SDSNHL), which was steroid dose dependent. We classified the patients into 2 groups: group A consisted of 6 patients with systemic SDSNHL, and group B consisted of 9 patients with inner-ear-specific SDSNHL without systemic disease. Group B patients were further classified as patients with slowly or rapidly progressive hearing loss. The yearly rate of hearing deterioration was greater in group B than in group A. Thus, the long-term hearing prognosis of patients in group B was worse than those in group A. Although SDSNHL may have immune-related origins, we hypothesize that hearing deterioration may be caused by proinflammatory cytokines because many of our cases exhibited abnormal immunological laboratory values and because many of these cases responded favorably to steroid treatment.

Introduction

Since autoimmune sensorineural hearing loss (AISNHL) was first reported by McCabe [McCabe, 1979], numerous studies have focused on investigating its clinical features, on determining its etiology, and on developing laboratory tests for its diagnosis [Harris and Sharp, 1990; Moscicki et al., 1994]. However, no specific diagnostic tests have been developed yet. Although long-term administration of steroids is the standard treatment for AISNHL, to the best of our knowledge, no reports exist on the long-term treatment outcome and prognosis of patients with AISNHL.

In 1975, we first reported a steroid-dependent case of AISNHL in a patient with Takayasu's arteritis (TA) [Kanzaki et al., 1975]. This disorder is an idiopathic chronic vasculitis that primarily affects large elastic arteries, such as the aorta and its major branches, and the pulmonary arteries [Kanzaki et al., 1975; Kerr et al., 1994]. Thereafter, we encountered patients with steroid-dependent hearing loss, but with no known systemic autoimmune disease. We termed these cases steroid-responsive sensorineural hearing loss (SNHL) [Kanzaki and O-Uchi, 1981, 1983]; however, we now prefer the term steroid-dependent sensorineural hearing loss (SDSNHL) and use this term in the present paper. SDSNHL may include AISNHL. However, the specific test for diagnosing AISNHL is not

KARGER
Fax +41 61 306 12 34
E-Mail karger@karger.ch
www.karger.com

1420–3030/09/0141–0026$26.00/0

Accessible online at:
www.karger.com/aud

Sho Kanzaki, MD, PhD
35 Shinanomachi, Shinjuku
Tokyo 160-8582 (Japan)
Tel. +81 3 5363 3827, Fax +81 3 3353 1261
E-Mail skan@sc.itc.keio.ac.jp

always available. Therefore, for the time being, we continue to diagnose SDSNHL based on the clinical course of the disease following steroid treatment.

We classified patients with SDSNHL into 2 subtypes: systemic [Kunihiro et al., 1990] and inner-ear-specific [Kanzaki, 1994a]. Systemic SDSNHL is associated with a systemic autoimmune disease, most frequently TA, whereas inner-ear-specific SDSNHL is not associated with any known systemic autoimmune disease, and is characterized by no clinical abnormalities other than hearing loss. Patients with systemic SDSNHL have a better prognosis than those with inner-ear-specific SDSNHL [Kanzaki, 1994a].

SNHL associated with TA is rare, and not all cases of SNHL associated with TA are steroid dependent. Although in Japan there is a significant number of reports of SNHL associated with TA, in other countries there are few reports of this disorder [Raza et al., 1998; Siglock and Brookler, 1987; Smith et al., 2004].

Because SDSNHL is rare and lacks a specific diagnostic test, it might be overlooked. If not diagnosed at an early stage and treated appropriately, SDSNHL may progress to profound hearing loss and may become unresponsive to steroid treatment. Thus, to diagnose SDSNHL at an early stage, physicians need to seriously consider the possibility that a patient presenting with hearing loss might have SDSNHL. Suspected cases should be treated immediately with steroids, which may be temporarily discontinued when hearing improves and resumed if the condition deteriorates. Thereafter, steroid treatment can be tapered off to a maintenance dose.

The purposes of the present study were to examine the long-term outcome of patients with SDSNHL, to determine whether the prognosis differs in patients with systemic SDSNHL associated with TA and those with inner-ear-specific SDSNHL, and to discuss the pathogenesis of SDSNHL. We followed these patients, on average, for over 10 years.

Subjects and Methods

The subjects were 15 patients with SDSNHL who have been under follow-up at the Department of Otorhinolaryngology, Keio University Hospital, since 1973. We classified the subjects into 2 groups: group A consisted of 6 patients with TA (systemic SDSNHL), and group B consisted of 9 patients with no known systemic autoimmune disease (inner-ear-specific SDSNHL).

Diagnosis of SDSNHL was based on previously described criteria [Kanzaki and O-Uchi, 1983] (table 1). We defined hearing deterioration as an elevation of the hearing threshold level by more than 15 dB in at least 2 consecutive frequencies.

Table 1. The criteria for the diagnosis of SDSNHL

A case of SNHL is determined to be definitely dependent on steroids when at least 1 of the following criteria are met:
(1) the sensorineural hearing loss improves with steroid administration, deteriorates upon discontinuation of the steroid, and improves again with resumption of the steroid
(2) the hearing loss deteriorates with tapering of the steroid dose and improves with increases in the steroid dose

Most of the subjects underwent pure-tone audiometry every month. More recently, the frequency of pure-tone audiometry testing was reduced to once every 2 months if a subject's hearing ability was stable and steroid dose was not tapered off. Subjects were advised to report to the hospital immediately if their hearing deteriorated.

All subjects underwent a routine screening panel for immunological diseases (serum IgG, IgM, IgA, complement, etc.). If the hearing loss deteriorated, the following blood tests were conducted: erythrocyte sedimentation rate (ESR); C-reactive protein serum levels; and serum positivity for perinuclear- and cytoplasm-antineutrophil cytoplasmic antibody, antinuclear antibody, and rheumatoid antigen. Hearing tests, otoacoustic emission (OAE), speech discrimination test, auditory brain stem response, and glycerol test were conducted according to the need of individual subjects. To examine vestibular function, we performed spontaneous, positional, and positioning nystagmus tests under an infrared charge-coupled device camera and caloric tests.

When SDSNHL was suspected, subjects were started on prednisolone (PSL) and Sairei-to therapy; Sairei-to is an herbal medicine believed to enhance the action of steroids [Kanzaki et al., 1993]. PSL was started at a daily dose of 30–40 mg. When hearing improved, the dose was decreased by 5 mg every 3–5 days. When we started to follow up these patients, it initially took about 4 months to reduce the PSL dose from 10 to 9 mg. More recently, however, we have increased this tapering-off period to 6 months. If a subject's hearing loss deteriorated while the PSL dosage was being decreased, we increased the dosage by 50%.

Results

All subjects were women. Subjects' ages and average hearing levels at the onset of hearing loss are shown in table 2. The mean ages at onset of hearing loss were 41 years (range: 37–45 years) for group A and 40.2 years (range: 11–60 years) for group B. The clinical course of hearing loss varied among the subjects. We assessed the subject's best hearing level, hearing level when hearing deteriorated during PSL weaning, and hearing level at the final examination.

Table 2. Clinical features of patients with SNHL

Case	Age at onset, years		Age, years		Response to steroid treatment			Onset pattern of deafness	Number of times hearing deteriorated	PSL dosage when hearing deteriorated, mg	Vertigo or dizziness
	right ear	left ear	first exam	final exam	response	no response	hearing in no-response ear				
Group A (systemic SDSNHL)											
1	45	35	45	53	right	left	total	rapid	4	0–4	no
2	39	39	39	40	right	left	mild	sudden	1	2.5	yes
3	46	–	48	51	right	–	normal	rapid	4	12.5–13	no
4	37	37	39	60	bilateral	–	–	rapid	5	2.5–8	no
5	–	42	42	60	left	–	normal	rapid	5	2–10	no
6	37	37	38	56	bilateral	–	–	gradual	6	2–8	no
Group B (inner-ear-specific SDSNHL)											
7	48	56	65	71	left	right	profound	rapid	3	0–3	no
8	48	47	48	61	right	left	total	gradual	4	3–15	no
9	34	30	34	50	right	left	total	rapid	6	8–13	yes
10	38	40	40	56	left	right	profound	rapid	4	0–13.5	no
11	47	40	48	53	bilateral	–	–	sudden	7	10–13	no
12	11	11	17	25	left	right	total	rapid	8	0–8	no
13	60	60	60	62	bilateral	–	–	rapid	4	6.5–9	no
14	29	28	29	34	bilateral	–	–	rapid	1	13	no
15	39	41	41	61	right	left	profound	sudden	6	5–9	no

Hearing levels were measured at 5 frequencies (250, 500, 1000, 2000, and 4000 Hz) and then averaged. Normal = Normal hearing; mild = sensorineural hearing loss; total = total deafness; profound = profound deafness.

Characteristics of Hearing Loss in Patients with Systemic Autoimmune Disease (Group A)

On average, patients in group A were followed for 158.0 months (range: 1 year 3 months to 21 years 11 months). For the 6 subjects of group A, the interval between hearing loss onset and their first hospital visit was 1 year or less for 3 subjects (cases 2, 4, 5) and from 1 to 2 years for the remaining 3 subjects (cases 1, 3, 6). Two subjects exhibited bilateral hearing loss, 3 subjects exhibited right-sided hearing loss, and 1 subject exhibited left-sided hearing loss. One subject experienced sudden onset of hearing loss, 4 subjects experienced rapid onset (although the exact date and time of onset could not be specified, hearing loss developed very rapidly, i.e. within 1 week), and 1 subject experienced gradual onset. Two subjects had normal hearing, 1 subject had moderate SNHL, and 1 subject had total deafness. Group A patients experienced sudden- or rapid-onset hearing loss when they were in their 30s or 40s and sought hospital treatment within 2 years of their hearing loss. Our first patient (case 1) was diagnosed with SDSNHL, and a definitive diagnosis of TA was made after she was referred to the department of internal medicine [Kanzaki et al., 1975; Kanzaki and O-Uchi, 1981]. The remaining 5 patients (cases 2–6) complained of hearing loss while they were being treated for TA in the department of internal medicine. These patients were subsequently referred to us for examination and diagnosed with SDSNHL. Two of these patients (cases 4, 6) had bilateral steroid-dependent hearing loss, 2 patients (cases 3, 5) had normal hearing in the contralateral ear, and 1 patient (case 2) had profound hearing loss in 1 ear and moderate hearing loss for high tones in the contralateral ear (table 3).

Characteristics of Patients with Inner-Ear-Specific Hearing Loss (Group B)

Patients in group B were followed for 136.8 months, on average (range: 2 years 4 months to 26 years 9 months; table 3). Of the 9 patients of group B, 12 ears were affected. The interval between onset and initial treatment was 1 year or less (prompt-treatment group average: 0.28 years) for 6 patients [7 ears affected: cases 8, 9, 10,11 (right), 13 (right), 14 (right and left)], whereas the interval between onset and initial treatment was more than 2 years (delayed-treatment group average: 4 years) for 4 patients [4 ears affected: cases 7, 11 (left), 12, and 15]. There were no significant differences in the rate of hearing deterioration between the prompt-treatment group (aver-

Table 3. Observation period and dosage of PSL at final examination and range of hearing changes during observation period

Case No.	Onset of hearing loss	Examination date				Hearing level (average of 5 frequencies)							
		first examinaion	final examination	observation period, years/ months	amount of PSL at final exam, mg	worst (a) dB	best (b) dB	final exam (c) dB	a–b dB	c–b dB	(c–b)/ years[1] dB	c–a dB	(c–a)/ years[1] dB
Group A (systemic SDSNHL)													
1		Feb 1973	Apr 1983	10/2	0	51	28	46	23	18	1.8	–5	0.6
2		Jan 1982	Apr 1983	1/3	0	87	32	47	55	15	11.5	–40	–32.0
3		Dec 1993	Mar 2005	10/3	2.5	64	45	63	19	18	1.7	–1	–0.1
4 (right)		Nov 1983	Sep 2006	21/11	12	54	13	34	41	21	1	–20	–0.9
4 (left)		Nov 1983	Sep 2006	21/11	12	47	30	41	17	11	0.4	–6	–0.3
5		Jan 1989	Sep 2006	16/9	8	48	20	24	28	4	0.2	–24	–1.4
6 (right)		Feb 1988	Sep 2006	18/8	10	68	19	70	49	51	2.9	2	0.1
6 (left)		Feb 1988	Sep 2006	18/8	10	63	19	38	44	19	1.1	–25	–1.4
Group B (inner-ear-specific SDSNHL)													
7	S	Jul 1983	Jan 1989	6/7	0	53	37	49	16	12	1.2	–4	–0.6
8	S	May 1977	Dec 1991	13/8	0	67	50	49	17	–1	0.07	–18	–1.3
9	R	Sep 1977	May 2003	26/9	8	77	13	91	64	78	3.2	14	0.5
10	S	Aug 1988	Mar 2004	15/8	0	67	32	54	35	22	1.4	–13	0.8
11 (right)	R	May 2000	Jan 2005	4/9	11	65	37	92	28	55	11.7	27	5.7
11 (left)	R	May 2000	Jan 2005	4/9	11	82	70	82	12	12	2.5	0	0.0
12	R	Sep 1981	Dec 1990	9/4	8	101	65	91	36	26	3.25	–10	–1.1
13 (right)	S	Nov 1979	Feb 1982	2/4	0	60	37	48	23	11	4.9	–12	–3.8
13 (left)	S	Nov 1979	Feb 1982	2/4	0	50	27	36	23	9	4	–14	–4.4
14 (right)	S	Jan 1985	May 1990	4/5	0	31	1	32	30	31	5.8	1	0.2
14 (left)	R	Jan 1985	May 1990	4/5	0	74	8	74	66	66	12.5	0	0.0
15	R	Jul 1987	Sep 2006	19/3	6	79	46	70	33	24	1.2	–9	–0.5

R = Rapid progressive hearing loss; S = slow progressive type.
[1] Observation years.

age: 5.65 dB/year) and delayed-treatment group (average: 2.43 dB/year; p = 0.13).

During the administration of the maintenance dose of PSL, hearing levels fluctuated before marked deterioration. There were no differences in the laterality of SDSNHL among subjects. Three subjects exhibited bilateral hearing loss, 3 subjects exhibited right-sided hearing loss, and 3 subjects exhibited left-sided hearing loss (table 2). Three subjects had profound hearing loss, and 3 subjects had total deafness (table 2). The onset pattern of hearing loss is shown in table 2. Two subjects experienced a sudden onset of hearing loss, 6 subjects experienced rapid onset, and 1 subject experienced gradual onset. Three patients (cases 11, 13, 14) had bilateral steroid-dependent hearing loss and the remaining 6 patients (cases 7, 8, 9, 10, 12, 15) had unilateral SDSNHL (table 3). At the time of their first visit to our department, these 6 patients had profound hearing loss or total deafness in the contralateral ear that was unresponsive to steroids.

OAE and Equilibrium Study

The speech discrimination test results of all the subjects were equivalent to those predicted from their pure-tone audiograms. OAE, including transient evoked otoacoustic emissions (TEOAE) and distortion product otoacoustic emissions (DPOAE), were examined in 8 subjects, 4 from group A and 4 from group B.

The four group A subjects had either normal hearing or moderate SNHL with TA. Of these 4 subjects, 2 had measurable TEOAE responses and 3 had measurable DPOAE responses. None of the 4 group B subjects showed responses. Only 1 group A subject and 1 group B subject experienced dizziness and canal paresis.

Weaning from PSL

Two group A subjects (cases 1, 2) and 5 group B subjects (cases 7, 8, 10, 13, 14) were successfully weaned from PSL. For the group A subjects, the average duration of PSL administration until weaning was 5 years 3 months